Research Article

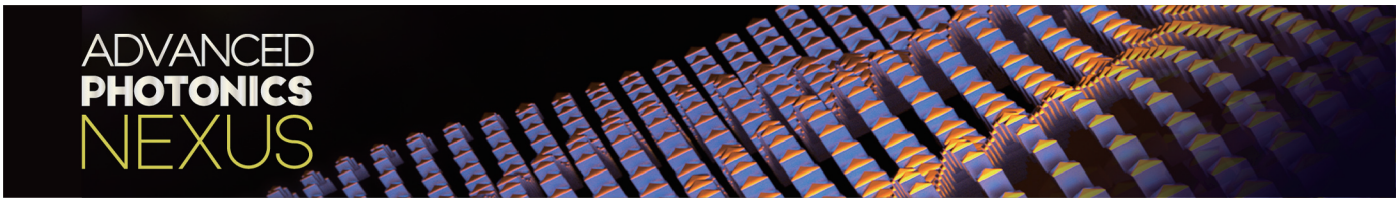

Characteristics of a Gaussian focus embedded within spiral patterns in common-path interferometry with phase apertures

Yizhou Tan[a,b] **and Ying Gu**[a,b,*]
[a]Chinese PLA General Hospital, the First Medical Center, Department of Laser Medicine, Beijing, China
[b]Hainan Hospital, Chinese PLA General Hospital, Laser Medicine Center, Sanya, China

Abstract. A phase-only method is proposed to transform an optical vortex field into desired spiral diffraction–interference patterns. Double-ring phase apertures are designed to produce a concentric high-order vortex beam and a zeroth-order vortex beam, and the diffracted intensity ratio of two beams is adjustable between 0 and 1. The coherent superposition of the two diffracted beams generates a brighter Airy spot (or Poisson spot) in the middle of the spiral pattern, where the singularity for typical vortex beam is located. Experiments employing circular, triangular, and rectangular phase apertures with topological charges from 3 to 16 demonstrate a stable, compact, and flexible apparatus for vortex beam conversion. By adjusting the parameters of the phase aperture, the proposed method can realize the optical Gaussian tweezer function and the optical vortex tweezer function simultaneously along the same axis or switch the experimental setup between the two functions. It also has potential applications in light communication through turbulent air by transmitting an orbital angular momentum-coded signal with a concentric beacon laser.

Keywords: finite aperture diffraction; phase-only beam transformation; orbital angular momentum; common-path interferometry; optical manipulation; light transmission through turbulent air.

Received Jan. 20, 2023; revised manuscript received Feb. 19, 2023; accepted for publication Mar. 8, 2023; published online Apr. 24, 2023.

[DOI: 10.1117/1.APN.2.3.036008]

1 Introduction

Optical waves carrying orbital angular momentums (OAMs) have been applied in optical manipulation, microscopy, quantum optics, and information encoding[1] since its first discovery by Allen et al. 30 years ago.[2] To expand the controllability of optical vortices, efforts have been made to modify the doughnut-shaped intensity distribution of the vortex beams, such as using the interference of Laguerre–Gaussian (LG) beams in a Mach–Zehnder interferometer to rotate optically trapped particles,[3] generating tiny dark spot diffraction of nonzero LG laser beams by an opaque disk,[4] generating continuously adjustable vortex beams by coaxial or small-angle interference,[5] using laser beams of different wavelengths incoherently overlaid to produce a sub-diffraction dark spot,[6] or generating concentric multirings by compound spiral phase plates.[7]

An important feature of the optical vortex beams is that the beam axis marks a singularity in the optical phase, and the amplitude of light becomes zero. Therefore, generating a bright Gaussian focus embedded with a spiral pattern remains challenging. Existing technology, such as computer-generated holograms, can generate a vortex beam of arbitrary patterns, including the diffraction–interference patterns studied in this work.[8,9] However, optical elements have to be carefully aligned in the holographic off-axis optical system, which makes it infeasible in long-term optical trapping with high positioning accuracy. Meanwhile, although a metasurface plate allows conversion of a polarized input beam into an arbitrary vortex mode, it is not possible to modify the operating parameters dynamically in a prefabricated metasurface.[10,11]

The generalized phase contrast (GPC) method converts a pattern of phase modulation into the corresponding intensity distribution.[12,13] Inspired by GPC, we propose a method for transforming an optical vortex field into the desired spiral

*Address all correspondence to Ying Gu, guyinglaser@sina.com

interferograms. Amplitude aperture is referred to as the hole on an optically opaque screen, and its diameter determines the diameter of the bundle of rays traversing through. Different from a triangular amplitude aperture, which produces a triangular lattice correlated with the topological charge of the vortex beam in the far-field plane,[14,15] we designed double-ring phase apertures to generate a concentric diffraction field. Based on the interference of the two diffraction fields, a sharp focus laser spot can be embedded into the middle of the spiral fringes.

Our experimental results have potential applications for micromanipulation: the measurements of torque, angle, and displacement of small objects such as enzymes link, protein binding, and DNA molecules require central trapping with rotation controls.[11,16] Verification of quantum entanglement needs the petal-like fringes containing a brighter reference point for the rotation angle identification, and twisted light transmission at long distances will need a concentric brighter beacon laser inside the encoded vortex beams to resolve the atmospheric turbulence problems.[17,18]

2 Principle

In this work, the experimental principle includes three main issues: the design of the double-ring phase-aperture, the diffraction theory for phase element, and the coherent combination between the vortex beam and Gaussian beam.[19–21]

2.1 Phase Only Transform

The double-ring phase-aperture is made of a transparent element which is divided into two parts: the inner circle zone of radius r_1 and the ring zone between r_1 and out radius r_2 , as shown in Fig. 1.

The double-ring phase-aperture is specially designed to realize three functions: (1) The element splits incident light at a designated ratio into two separate subbeams with phase difference. (2) The helical phase modulation profile, covered on the local zone, is able to generate a subbeam carrying OAM. (3) Diffraction patterns in the far-field are created by finite aperture diffraction. In the rest of this work, the double-ring phase-aperture element is frequently referred to as "phase aperture" for short.

The beam conversion process is shown in Fig. 1. In the far-field, the diffracted intensity distribution $I_p(x,y) = |E_p(x,y)|^2$. The diffracted electric field distributions $E_p(x,y)$ for the circular aperture (annular and polygon aperture) are expressed by Eqs. (S1)–(S4) in the Supplemental Material. Full details of the diffraction-interference calculation for vortex beams are given in the Supplemental Material.

2.2 Common-Path Interference Scheme

In our experiments, one zone of the double-ring phase-aperture element is covered with the helical phase modulated profile $\exp(il\theta)$ with the topological charge l and the azimuthal angle θ, and the other zone has a uniform phase profile.

When a plane wave beam passes through the double-ring phase apertures, the incident beam is split into high-order vortex beam A and zeroth-order vortex beam B. A simple and compact optical interference setup is shown in Fig. 1 and Fig. S1 in the Supplemental Material, in which the subbeam A and concentric subbeam B travel along essentially the same path.[20,22,23]

2.3 Interference between Two Diffraction Fields

The compound patterns, such as the Gaussian laser focus embedded with spiral petal-like fringes, are observed. We explain the physical reasons behind this result based on the theoretical model: (1) Both the vortex beam and the plane wave (or Gaussian laser) beam are converted into Fraunhofer diffraction fields through a finite aperture. (2) The coherent superposition of two diffraction fields generates interference fringes in the far-field.

Case I: The inner circle zone outputs a vortex beam, and the circular phase aperture generates the diffraction electric distribution $E_{\text{circular}}(x,y)$ in the far-field. The ring zone without phase modulation outputs a Gaussian beam. The annular phase aperture generates the diffraction electric field $E_{\text{annular}}(x,y)$ in the far-field, which creates the Poisson diffraction spot on the optic axis, as shown in Fig. S1(e) in the Supplemental Material.[4,24] In Fig. 1(a), when the coherent superposition between $E_{\text{circular}}(x,y)$ and $E_{\text{annular}}(x,y)$ occurs in the far-field, the resulting compound pattern is a spiral petal-like fringe with the brighter Poisson spot in the middle.

Case II: The circular inner zone outputs a Gaussian beam, which generates the diffraction electric distribution $E_{\text{circular}}(x,y)$ with a brighter spot on the optic axis, called an Airy spot

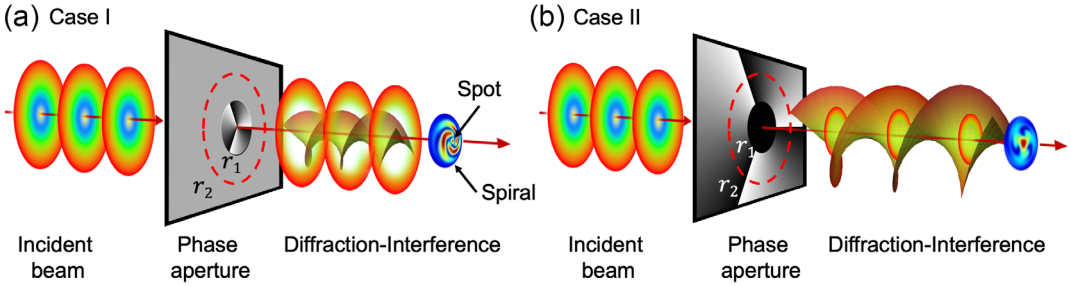

Fig. 1 Interference between diffracted vortex beam and diffracted plane wave beam through a phase aperture in common-path interferometry. (a) Case I: the inner circle zone ($\leq r_1$) is covered with the helical phase-modulated profile $\exp(il\theta)$ with the topological charge $l = 3$. The ring zone ($\geq r_1, \leq r_2$) is without phase modulation and outputs a Gaussian beam. (b) Case II: the circle zone ($\leq r_1$) is without phase modulation. The ring zone ($\geq r_1, \leq r_2$) is covered with the helical phase-modulated profile $\exp(il\theta)$ with the topological charge $l = 3$.

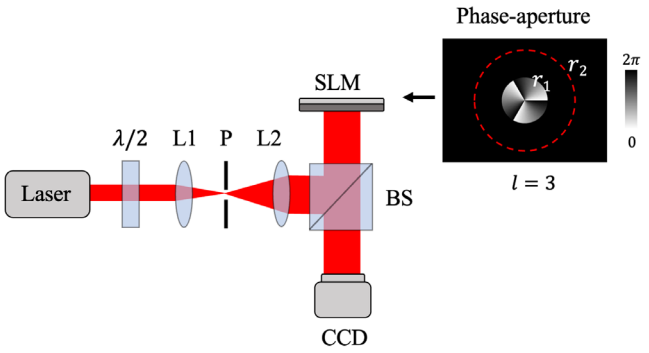

Fig. 2 Experimental setup of common-path interferometry with a phase aperture. $\lambda/2$, half-wavelength plate; L1, L2, lens; P, pinhole; BS, beam splitter; SLM, spatial light modulator; CCD, charge-coupled device. r_1 is the inner radius of the phase aperture, r_2 is the outer radius of the phase aperture indicated by red dashed line.

in Fig. S1(i) in the Supplemental Material. The ring zone outputs a vortex beam, which generates the diffraction electric field $E_{\text{annular}}(x, y)$ in the far-field. The coherent superposition between $E_{\text{circular}}(x, y)$ and $E_{\text{annular}}(x, y)$ results in a compound pattern in the far-field, which has propeller-like fringes with the brighter Airy spot in the middle in Fig. 1(b).[20,21,25]

A noticeable feature in our method is that a brighter Airy spot (Poisson spot) can automatically align with the center of the vortex beam all the time, which is attributed to the coherent combination of the vortex beam and the concentric Gaussian beam.

In this section, we analyze the theory and method for shaping the light optical wavefront by employing a transmissive spatial light modulator (SLM). The transmission-mode SLM is a necessary condition for realization of common-path interference in Fig. 1 and Fig. S1 in the Supplemental Material.

In following experimental study, we employ the reflection-mode SLM to demonstrate the diffraction-interference theory for vortex beams.

3 Experimental Setup

The experimental arrangement is shown in Fig. 2. The light beam from an He–Ne laser ($\lambda = 632.8$ nm) passes through a $\lambda/2$ plate that changes its polarization direction. The beam is then expanded by lenses L1 and L2 to fulfill the reflection area of the SLM (resolution, 1920×1080; effective area, 15.36 mm $\times$ 8.86 mm). A pinhole (P) is inserted to remove any other higher-order diffracted term. The incident light is redirected to illuminate the SLM vertically. The designed circular phase aperture is loaded onto the SLM. The modulated beam is recorded by a CCD camera, which is placed on the image plane.

4 Results

4.1 Beam Transformation through a Circular Phase Aperture in Common-Path Interferometry

To verify the feasibility of generating spiral petal-like fringes with a Gaussian focus in the middle, two experiments have been carried out. The experimental conditions correspond to Case I and Case II in Sec. 2.

In Experiment I, a transparent phase-aperture element is designed. The internal circle zone has an $\exp(il\theta)$-modulated phase profile of $l = 3$, and the ring zone has a uniform phase profile. The combination of the two profiles, which is loaded onto the SLM, is shown in Fig. 3(a).

The phase-modulated SLM produces a concentric beam in the Fresnel region: the inner is a vortex beam with a circular cross section, and the outer beam is a plane-wave beam with an annular cross section.

The interference between the diffraction fields of the vortex beam and the plane wave occurs in the far-field. Numerical calculations of the interference fringe are performed according to the theoretical model in Sec. 2 and Eqs. (A1)–(A4) in the Supplemental Material. The simulated intensity two-dimensional (2D)-distribution is shown in Fig. 3(b). A three-lobe spiral pattern with a brighter spot in the middle was observed in Fig. 3(c). The experimentally recorded interference fringe is in agreement with the numerical calculation result.

In Experiment II, a transparent phase-aperture element is designed. The internal circle zone has a uniform phase profile, and the ring zone has an $\exp(il\theta)$-modulated phase profile of $l = 3$. The combination of the two profiles is shown in Fig. 3(d). In the Fresnel region, the inner plane-wave beam has a circular cross section, and the outer vortex beam has an annular cross section. The diffraction–interference pattern is shown in Fig. 3(e) for the calculation result, and in Fig. 3(f) for the experimental result. We observed a three-arm propeller-like pattern with a strong light focus in the middle.

4.2 Beam Transformation through a Triangular Phase Aperture in Common-Path Interferometry

To verify the diffraction–interference effect of the triangular phase aperture, two experiments have been carried out.

In Experiment I, a transparent phase-aperture element is designed: the inner triangle zone has an $\exp(il\theta)$-modulated phase profile of $l = 3$, and the zone between the inner triangle and the outer ring has a uniform phase profile. The combination of two profiles, which is loaded onto the SLM, is shown in Fig. 4(a). The phase-modulated SLM produces a concentric beam in the Fresnel region: the inner is a vortex beam with a triangular cross section, and the outer is a dark hollow plane-wave beam. The interference between the diffraction fields of the vortex beam and the plane wave occurs in the far-field. The 2D distributions of the diffraction–interference pattern is numerically simulated; the result is shown in Fig. 4(b). The experimental result is shown in Fig. 4(c). A three-lobe spiral pattern with a brighter spot in the middle was observed.

In Experiment II, a transparent phase-aperture element is designed: the inner circle zone has a uniform phase profile, and the zone between the inner triangle and the outer ring has an $\exp(il\theta)$-modulated phase profile of $l = 3$. The combination of the two profiles is shown in Fig. 4(d).

In the Fresnel region, the inner plane-wave beam has a triangular cross section, and the outer beam is dark hollow vortex beam. Numerically simulated 2D distributions of the diffraction–interference pattern is shown in Fig. 4(e) and the experimentally recorded intensity distribution is shown in Fig. 4(f). A three-arm Y-shaped pattern with a brighter spot in the center of the interference fringe was observed.

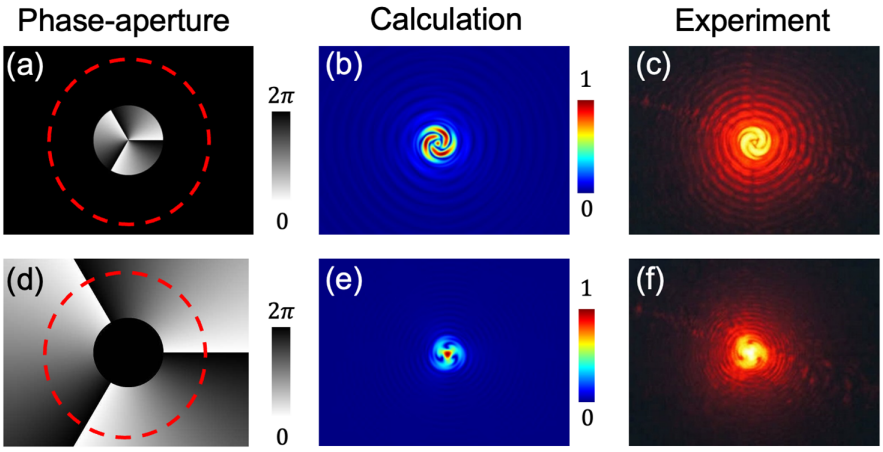

Fig. 3 (a) Circular phase-aperture element with a helical phase-modulated profile in the inner circle zone. (b) Numerically simulated light intensity distribution modulated by (a). (c) Experimentally recorded intensity distribution modulated by (a). (d) Circular phase-aperture element with a helical phase-modulated profile in the ring zone. (e) Numerically simulated light intensity distribution modulated by (d). (f) Experimentally recorded intensity distribution modulated by (d). The red dashed circle indicates the outer radius r_2 of the phase aperture.

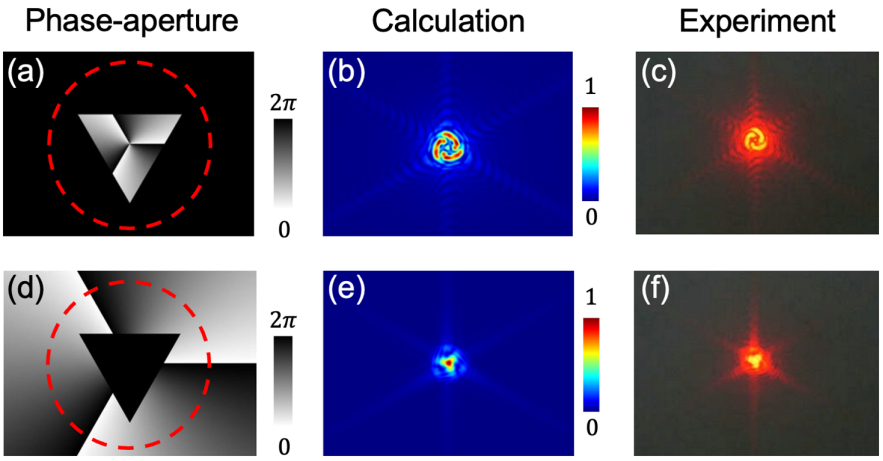

Fig. 4 (a) Triangular phase-aperture element with a helical phase-modulated profile in the inner zone. The inner equilateral triangle has the side length d. (b) Numerically simulated intensity distribution modulated by (a). (c) Experimentally recorded intensity distribution modulated by (a). (d) Circular phase-aperture element with a helical phase-modulated profile in the zone between the inner triangle and outer ring. (e) Numerically simulated intensity distribution modulated by (d). (f) Experimentally recorded intensity distribution modulated by (d). The red-dashed circle indicates the outer radius r_2 of the phase aperture.

4.3 Effect of Phase Aperture Size on the Diffraction–Interference Pattern

Next, we study the effect of the size of the phase aperture on the diffraction–interference pattern. The side length d of the triangular phase aperture is set to 100, 300, 600, and 900 pixels (the SLM width is 1080 pixels in our experiment). By adjusting the side length d, we observed the revolving of the diffraction–interference patterns from a Gaussian spot to a doughnut-shaped intensity pattern; results are shown in Fig. 5.

The effect of the size of the circular and rectangular phase apertures on the diffraction–interference pattern is plotted in Fig. S2 in the Supplemental Material.

4.4 Rotating the Diffraction–Interference Pattern

The orientation of diffraction–interference pattern is turned by the following methods.

In the first experiment, the helically modulated phase profile stays constant. Meanwhile, the direction of the triangular phase

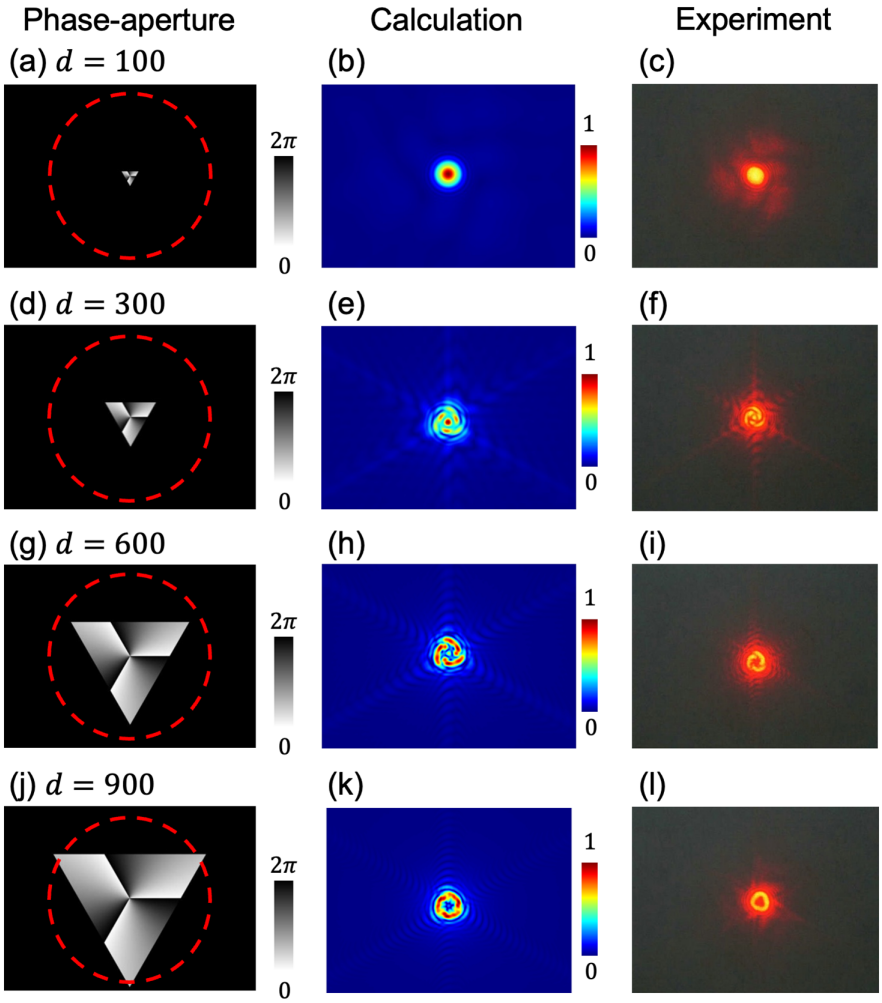

Fig. 5 (a), (d), (g), (j) Triangular phase-aperture element with a helical phase-modulated profile in the inner zone. The triangular phase aperture has a different side length, d. (b), (e), (h), (k) Numerically simulated intensity distribution and (c), (f), (i), (l) experimental intensity distribution in the far-field. The red dashed circle indicates the outer radius r_2 of the phase aperture.

aperture is rotated around the optical axis of the phase-aperture element, as shown in Figs. 6(a), 6(d), 6(g), and 6(j). The numerically simulated intensity 2D distribution and recorded intensity distribution demonstrated that the diffraction–interference pattern rotates in a clockwise direction. Results are shown in Fig. 6.

In the previous experiment, the phase shift in the outer zone of the phase aperture is set to 2π. In the following experiments, the phase shift of the outer area of the triangular phase aperture equals 0, as shown in Fig. 7(a). The interference fringe is shown in Fig. 7(b) for calculation and in Fig. 7(c) for the experiment. To test the effect of the phase shift on the orientation of the diffraction–interference pattern, the phase shift is set to π in the outer zone, represented by the gray area in Fig. 7(d). We found that the orientation of interference fringe tilted 60 deg. The calculation and experimental results are shown in Figs. 7(e) and 7(f), respectively.

4.5 *Effect of Phase Aperture Shape and Topological Charge on the Diffraction–Interference Pattern*

The relationship between the shape of the phase aperture and the topological charge l is studied. A phase aperture with an inner triangular zone containing $l = 4$ and $l = 8$ is loaded onto the SLM, as shown in Figs. 8(a1) and 8(b1). Spiral petal-like diffraction shapes with four and eight lobes were observed with asymmetric energy distribution; the results are shown in Figs. 8(a2) and 8(a3) and Figs. 8(b2) and 8(b3), and the Gaussian spot was not observed in the middle of the pattern. A phase aperture with an inner rectangular zone containing $l = 4, 8, 16$ is loaded onto the SLM separately. Spiral petal-like diffraction–interference patterns of 4, 8, and 16 lobes with a bright spot in the center were observed and are shown in Figs. 8(c), 8(d), and 8(e), respectively.

5 Discussion

5.1 *Integration of Optical Trapping Function and Controllable Rotation Function*

In optical Gaussian tweezers, a tightly focused Gaussian laser beam generates a trapping force that can capture and move small particles under a microscope.[26,27] In an optical tweezers employed vortex beam, micrometer particles can be rotated by the twisting force originating from OAM.[3,28,29]

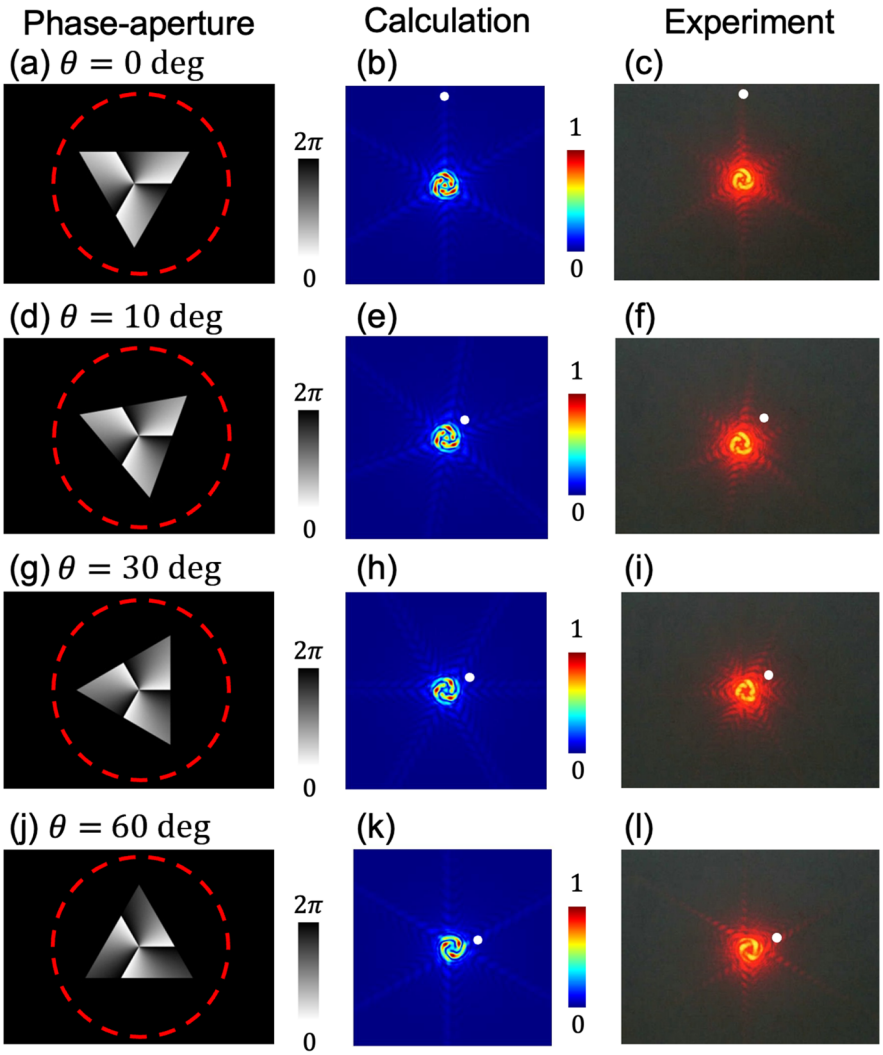

Fig. 6 (a), (d), (g), (j) Triangular phase-aperture element with a helical phase-modulated profile inside. The orientation of the triangular phase aperture tilts with different angle θ; the angle $\theta = 10$ deg, 30 deg, 60 deg. (b), (e), (h), (k) Numerically simulated intensity distribution and (c), (f), (i), (l) experimentally generated intensity pattern. *The white dots indicate the changed direction of the interference fringes. The red dashed circle indicates the outer radius r_2 of the phase aperture.

Owing to the different roles of optical Gaussian tweezers and optical vortex tweezers, each of them could not be replaced by another.[3,30] To investigate and control rotational motion of small particles, it is necessary to develop a compact device that combines an optical trapping function with a controllable rotation function.[30–32]

We demonstrated that our experimental setup is able to generate three kinds of light intensity distributions: a tightly focused spot, a spiral petal-like fringe, and a doughnut-shaped fringe, which stay at the same center line. The phase-only transform method in our work supports a concept of optical tweezers that integrates the optical Gaussian tweezers and optical vortex tweezers in a single optical system.

By adjusting the inner size of the phase aperture, the light intensity distributions gradually evolve from a tightly focused spot to a doughnut-shaped fringe, as shown in Fig. 5 and Fig. S2 in the Supplemental Material. The experimental results are in good agreement with the theoretical calculation results.

For the side length of a triangular phase aperture $d = 100$ pixel, the helical phase-modulated pattern occupies about 10% of the effective modulation area, and the intensity distribution at the far-field is closed to a Gaussian focal spot, as shown in Figs. 5(b) and 5(c). While the side length d increases, more light carries OAM information and a three-armed spiral fringe appears, as shown in Figs. 5(e) and 5(f) and Figs. 5(h) and 5(i). When $d = 900$ pixel, which occupies nearly 90% of the phase modulation area due to the dominant contribution of the vortex beam, the light intensity distribution is expanded to a doughnut-shaped pattern, as shown in Figs. 5(k) and 5(l).

To achieve symmetric energy distribution with a bright center, a triangular phase aperture with even topological charges

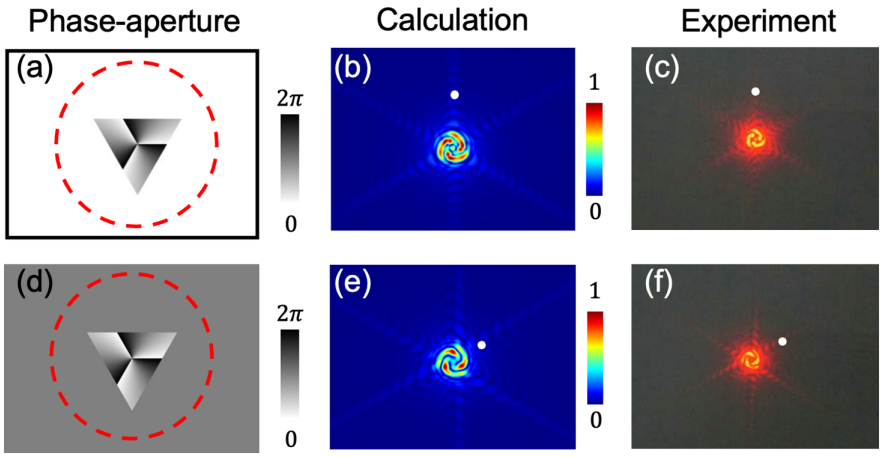

Fig. 7 (a) Triangular phase-aperture element with a helical phase-modulated profile inside. The outer zone of the phase aperture has 0 phase shift. (b) Numerically simulated intensity distribution. (c) Experimental recording. (d) The outer zone of the phase aperture has π phase shift. (e) Numerically simulated intensity distribution. (f) Experimental recording. The white dots indicate the changed direction of the interference fringes. The red dashed circle indicates the outer radius r_2 of the phase aperture.

or a rectangular phase aperture with odd topological charges is necessary.[14,15] When an even topological charges phase-modulated profile is loaded inside a triangular phase aperture, the interference fringe is asymmetric, and the central bright spot is either missing or weak, as shown in Figs. 8(a) and 8(b).[33] While the circular phase aperture generates symmetric energy distribution in every lobe, it is difficult to distinguish the rotation, which will be discussed in the following section.

5.2 Rotate the Orientation of Diffraction–Interference Pattern by Adjusting the Phase Aperture

This work studies two strategies to rotate the orientation of diffraction–interference pattern. First, we explore the possibility of controlling rotation by turning the orientation of the triangular phase aperture. As shown in Fig. 6, the orientation of the triangular phase aperture is rotated by steps, with the orientation of the diffraction–interference pattern rotated accordingly.

The existing method rotates the orientation of the pattern by changing the optical path.[3,16] By comparison, our approach realized concentric rotation of the diffraction–interference pattern of the optical vortex by adjusting the geometric variable only.[3,16]

Second, we show that the phase shift of a triangular phase aperture affects the orientation of the diffraction-interference pattern. By comparison, the phase shift of 0 [Figs. 4(b) and 4(c)] and 2π [Figs. 7(b) and 7(c)] generates exactly same light intensity distributions. However, the phase shift π rotates the direction of the diffraction-interference pattern around the optic axis in Figs. 7(e) and 7(f). A φ phase change in the wavefront will cause the diffraction–interference pattern to rotate by φ/l, which is 60 deg in Figs. 7(e) and 7(f). The effect is similar to a Guoy phase shift observed in a Mach–Zehnder interferometer (MZI).[1,16,34]

5.3 Potential Application in Optical Communication

To compensate for small perturbations in optical communication, a vortex beam carrying encoded OAM has been transformed into a 3×3 grid with $l = 0$ component in the center as the measurement.[35] We demonstrates optical transmission with a topological charge values $l = 4, 8, 16$ using a rectangular phase aperture, which automatically embedded the diffraction fringe with a Gaussian spot for reference in Figs. 8(c)–8(e).

Long-distance twisted light transmission experiments have been realized, and the transmission quality of the OAM modes was primarily reduced due to atmospheric turbulence near the sender.[17,18] The literature[18] proposed employing a second laser beam to create a guide star.[18] Our method is able to generate a Gaussian spot that can be used as the beacon laser with OAM-encoded information simultaneously in a simple optical setting.

5.4 Comparison between Optical Conversion Methods

Both computer-generated holograms and conventional MZIs are able to generate spiral petal-like patterns, which are similar to the patterns reported in this work.[3,8,9,34] A holographic system is able to generate arbitrary patterns, but the zero-order diffracted beam is not used, which inevitably wastes incident optical power. Meanwhile, the holographic optical elements need to be carefully aligned due to the shortcomings of the off-axis optical system, making it unfeasible in long-time stable optical trapping.[8,9]

The MZI is the most common way to modulate intensity patterns of an optical vortex field. However, misalignment during interference may cause unsatisfactory interference fringes. And 50:50 splitting incident beam decreases its light conversion efficiency.[3,20,21,34]

In terms of fulfilling the special requirement, such as new concepts of optical tweezers and laser beacon in turbulent air (or as a reference point for OAM-coded pattern recognition), the common-path interferometer with a double ring phase aperture has advantages in various applications. For instance, it can work in a vibrating or noisy environment with relatively simple and compact optical setups. The transmissive phase-only element has high conversion efficiency. The double ring phase-aperture

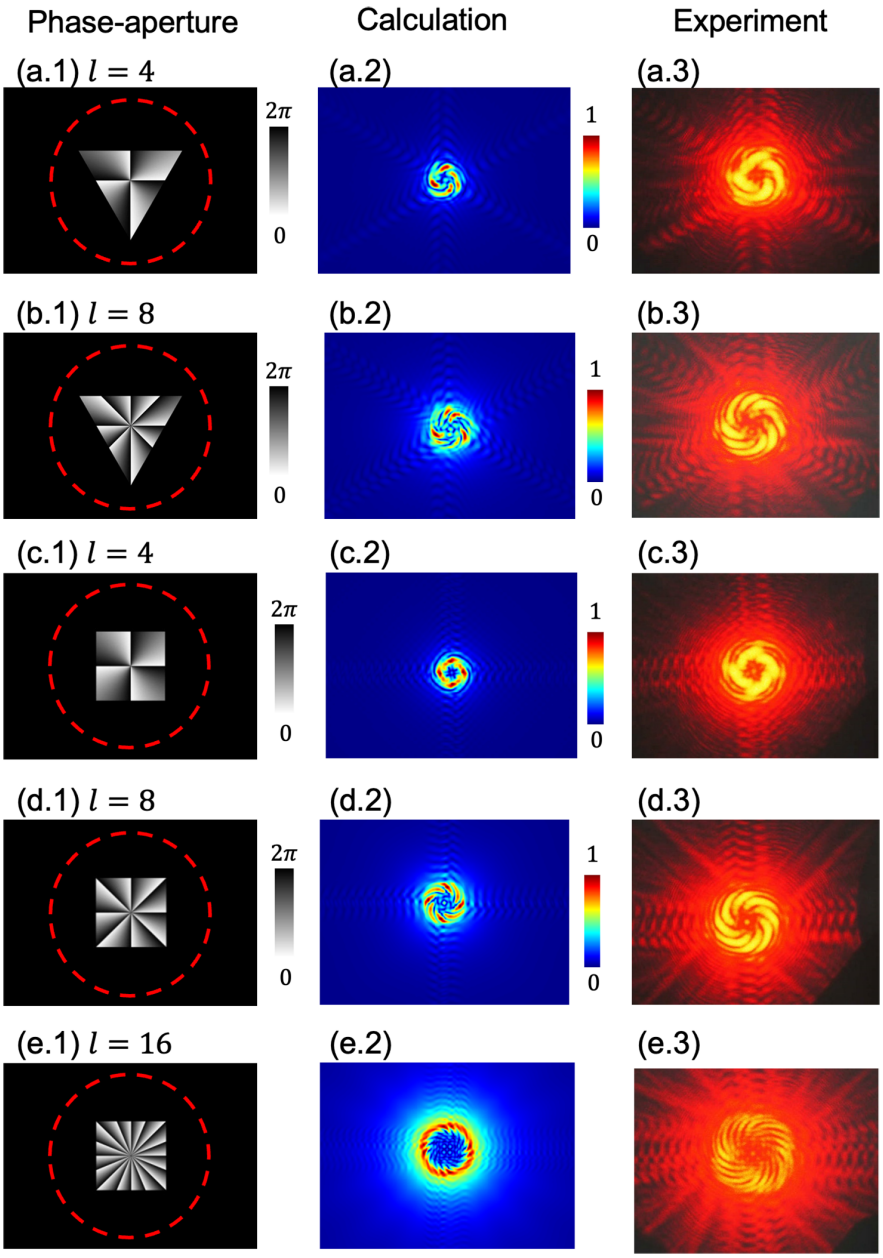

Fig. 8 (a), (b) Triangular phase aperture with a helical phase-modulated profile inside ($l = 4$ and $l = 8$). (c)–(e) Rectangular phase aperture with a helical phase-modulated profile inside ($l = 4, 8, 16$). The red dashed circle indicates the outer radius r_2 of the phase aperture. The first column illustrates the phase modulation profile; the second column shows the calculated light intensity distribution, and the third column shows the experimental results.

element produces concentric beams, which allow dynamical parameter adjustment of optical vortex fringes along the same axis; details are given in Sec. 4.[36–38]

6 Conclusion

This work proposes a phase-only method for transforming an optical vortex field into a desired spiral interference fringe. By employing double ring phase-aperture elements to realize common-path interference, a brighter spot is embedded with the optical vortex fringe. The embedded spot is located the singularity of the typical vortex beam is. In theory, this type of brighter spot originates from an Airy spot (or Poisson spot) due to the zeroth-order vortex beam diffracted at the phase aperture. A noticeable feature is that the brighter spot is automatically aligned with the central axis of the vortex beam because it is attributed to the coherent combination of vortex beam and concentric Gaussian beam. The theoretical calculated patterns are in excellent agreement with diffraction–interference fringes in experiment. Our experimental setup offers a method to implement optical tweezers that can trap and twist a particle (or biological sample) spatially and angularly. By controlling the phase

shift and the size of the circular or polygonal phase aperture, the intensity distributions in the far field are able to evolve from a doughnut shape to a Gaussian focus, and the orientation of the diffraction–interference pattern can be rotated and controlled.

Acknowledgments

This work was supported by the National Natural Science Foundation of China (Grant Nos. T2293753 and T2293750) and the Major Science and Technology Project in Hainan Province of China (Grant No. ZDKJ2019012).

References

1. M. Padgett and R. Bowman, "Tweezers with a twist," *Nat. Photonics* **5**, 343–348 (2011).
2. L. Allen et al., "Orbital angular momentum of light and the transformation of Laguerre-Gaussian laser modes," *Phys. Rev. A* **45**, 8185–8189 (1992).
3. L. Paterson et al., "Controlled rotation of optically trapped microscopic particles," *Science* **292**, 912–914 (2001).
4. O. Emile et al., "Dark zone in the centre of the Arago-Poisson diffraction spot of a helical laser beam," *Europhys. Lett.* **101**, 54005 (2013).
5. J. Qi et al., "Continuously adjustable cylindrical vector and vortex beams by programming vortex half-wave plates and detection based on coaxial or small-angle interference," *Phys. Rev. Appl.* **18**, 034086 (2022).
6. C. Li et al., "Analytical description of sub-diffraction dark spot," *Opt. Commun.* **499**, 127295 (2021).
7. X. Liu et al., "Coaxial multi-ring optical vortex generation based on compound spiral phase plates," *Laser Phys.* **32**, 035402 (2022).
8. J. E. Curtis, B. A. Koss, and D. G. Grier, "Dynamic holographic optical tweezers," *Opt. Commun.* **207**, 169–175 (2002).
9. J. E. Curtis and D. G. Grier, "Modulated optical vortices," *Opt. Lett.* **28**, 872–874 (2003).
10. M. Piccardo and A. Ambrosio, "Arbitrary polarization conversion for pure vortex generation with a single metasurface," *Nanophotonics* **10**, 727–732 (2020).
11. T. Li et al., "Multidimensional light field manipulation and applications based on optical metasurface," *Proc. SPIE* **11850**, 1185004 (2021).
12. D. J. Lee and A. M. Weiner, "Optical phase imaging using a synthetic aperture phase retrieval technique," *Opt. Express* **22**, 9380–9394 (2014).
13. W. Chi and N. George, "Phase-coded aperture for optical imaging," *Opt. Commun.* **282**, 2110–2117 (2009).
14. J. M. Hickmann et al., "Unveiling a truncated optical lattice associated with a triangular aperture using light's orbital angular momentum," *Phys. Rev. Lett.* **105**, 053904 (2010).
15. L. E. de Araujo and M. E. Anderson, "Measuring vortex charge with a triangular aperture," *Opt. Lett.* **36**, 787–789 (2011).
16. M. P. MacDonald et al., "Revolving interference patterns for the rotation of optically trapped particles," *Opt. Commun.* **201**, 21–28 (2002).
17. M. Krenn et al., "Communication with spatially modulated light through turbulent air across Vienna," *New J. Phys.* **16**, 113028 (2014).
18. M. Krenn et al., "Twisted light transmission over 143 km," *Proc. Natl. Acad. Sci. U. S. A.* **113**, 13648–13653 (2016).
19. F. Kenny et al., "Adaptive optimisation of a generalised phase contrast beam shaping system," *Opt. Commun.* **342**, 109–114 (2015).
20. J. Glückstad and P. C. Mogensen, "Optimal phase contrast in common-path interferometry," *Appl. Opt.* **40**, 268–282 (2001).
21. A. Ustinov et al., "Focal-plane field when lighting double-ring phase elements," *Comput. Opt.* **41**, 515–520 (2017).
22. A. Bañas and J. Glückstad, "Light shaping with holography, GPC and holo-GPC," *Opt. Data Process. Storage* **3**, 20–40 (2017).
23. D. Palima and J. Glückstad, "Generalised phase contrast: microscopy, manipulation and more," *Contemp. Phys.* **51**, 249–265 (2010).
24. P. Fischer et al., "The dark spots of Arago," *Opt. Express* **15**, 11860–11873 (2007).
25. C. Jun, K. Deng-Feng, and F. Zhi-Liang, "Properties of Fraunhofer diffraction by an annular spiral phase plate for sidelobe suppression," *Chin. Phys. Lett.* **26**, 094210 (2009).
26. A. Ashkin, J. M. Dziedzic, and T. Yamane, "Optical trapping and manipulation of single cells using infrared laser beams," *Nature* **330**, 769–771 (1987).
27. A. Ashkin and J. M. Dziedzic, "Optical trapping and manipulation of viruses and bacteria," *Science* **235**, 1517–1520 (1987).
28. V. Shahabadi and E. Madadi, "Effective multiple optical trapping of sub-micrometer particles with petal beams," *J. Opt. Soc. Am. B* **37**, 3665 (2020).
29. S. P. Kotova et al., "Manipulation of microscopic objects with two-lobe light fields," *Bull. Lebedev Phys. Inst.* **49**, 362–365 (2022).
30. F. Pedaci et al., "Excitable particles in an optical torque wrench," *Nat. Phys.* **7**, 259–264 (2011).
31. A. La Porta and M. D. Wang, "Optical torque wrench: angular trapping, rotation, and torque detection of quartz microparticles," *Phys. Rev. Lett.* **92**, 190801 (2004).
32. C. Deufel et al., "Nanofabricated quartz cylinders for angular trapping: DNA supercoiling torque detection," *Nat. Methods* **4**, 223–225 (2007).
33. A. Ambuj et al., "Symmetry in the diffraction of beams carrying orbital angular momentum," *Phys. Rev. A* **99**, 013846 (2019).
34. H. Huang et al., "Phase-shift interference-based wavefront characterization for orbital angular momentum modes," *Opt. Lett.* **38**, 2348–2350 (2013).
35. G. Gibson et al., "Free-space information transfer using light beams carrying orbital angular momentum," *Opt. Express* **12**, 5448–5456 (2004).
36. S. W. Hell and J. Wichmann, "Breaking the diffraction resolution limit by stimulated emission: stimulated-emission-depletion fluorescence microscopy," *Opt. Lett.* **19**, 780–782 (1994).
37. G. Vicidomini, P. Bianchini, and A. Diaspro, "STED super-resolved microscopy," *Nat. Methods* **15**, 173–182 (2018).
38. M. J. Villangca et al., "Dark GPC: extended nodal beam areas from binary-only phase," *Opt. Eng.* **55**, 125102 (2016).
39. A. Ambuj, R. Vyas, and S. Singh, "Diffraction of orbital angular momentum carrying optical beams by a circular aperture," *Opt. Lett.* **39**, 5475 (2014).
40. R. Vasilyeu et al., "Generating superpositions of higher-order Bessel beams," *Opt. Express* **17**, 23389–23395 (2009).

Yizhou Tan is an assistant researcher at Chinese PLA General Hospital. He received his BS and MS degrees from the National University of Defense Technology in 2011 and 2013, respectively, and his PhD in physics from Cavendish Laboratory, Cambridge University, in 2018. His current research focuses on laser medicine and its clinical application.

Ying Gu: Biography is not available.